

EXPERIMENTAL DETERMINATION OF TUNNEL VENTILATION AXIAL DUCTED FAN PERFORMANCE

by

Milan B. ŠEKULARAC

Laboratory for Turbulent Flows, Faculty of Mechanical Engineering,
University of Montenegro, Podgorica, Montenegro

Original scientific paper
DOI: 10.2298/TSCI140624108S

To investigate traffic tunnel ventilation flows, a scaled model of a traffic tunnel with longitudinal ventilation system based on ducted fans is used. Flows in tunnels are influenced by tunnel geometry, fan characteristics, ventilation operation scenario, vehicle traffic, atmospheric factors, etc. To analyze flow fields of tunnels in detail, knowledge of tunnel jet-fan properties and turbulent flow characteristics at the fan exit are required, and can be used as input data for computer fluid dynamics boundary conditions of tunnel flow computation. For this purpose experimental measurements were done using the hot wire anemometry technique. The obtained results, through ensemble-averaged and time averaged profiles of all velocity components, turbulence intensity, turbulent kinetic energy, integral flow length scales, available Reynolds stresses, turbulent kinetic energy production rates, and the fan thrust performance, are presented. These data allow us to analyze in more detail the influence of fan flow on energy and pollutant removal efficiencies of the tunnel ventilation and to evaluate accuracy of computer fluid dynamics studies on fan improvements.

Key words: *ventilation, traffic tunnel, ducted fans, unmanned aerial vehicle fan, turbulence*

Introduction

Longitudinally ventilated traffic tunnels mostly utilize ventilation systems based on axial ducted (jet) fans attached to the tunnel ceiling. For conducting experimental research of this problem, a scaled model of traffic tunnel with longitudinal ventilation presented in fig. 1 is utilized. Details about tunnel model installation characteristics can be found in [1]. Geometric similarity of the model tunnel and real scale tunnel has a scale ratio of 1:19. Since Reynolds number equality condition cannot be satisfied, experimental results cannot be used in quantitative way to analyze real scale tunnel ventilation system. Using this model the influence of the flow characteristics at the fan exit which are the boundary conditions for CFD model can be studied in detail. If it happens that any of these characteristics play a significant role on the flow field or pollutant dispersion in this model, one can expect similar influence on the real flow systems. Moreover, complete similarity conditions between laboratory and CFD model can be reached by choosing a virtual fluid with viscosity scaled to satisfy the equality of Reynolds number. Special concern of this current research is also the mechanical efficiency of the ventilation, and its improvement possibilities, [1-3]. To carry this research task, a



Figure 1. Traffic tunnel laboratory installation tests

detailed experimental and numerical assessment of both fan-flow and tunnel-flows is necessary. The laboratory model can also be used to validate 1-D numerical models for ventilation design, which also requires some of the fan characteristics, studied here. Different axial fan configurations could be found in tunnels: ducted fans, ducted fans with silencers, reversible or unidirectional, fans with slanted wings or slanted silencers (banana jet), and fans with slanted converging nozzles, [2, 3]. To be able to carry out detailed CFD analysis of tunnel flows, ventilation scenarios and the pollutant removal efficiency, a detailed insight in the fan flow field is required.

The experimental results presented here will support further evaluation of fan induced flow effects in the tunnel on the overall energy and pollutant transport efficiencies.

Ducted fan flow field is characterized by complex structure, with transient periodic appearance. This periodicity originates from rotor blades' rotational motion. Complex structure of turbulence is produced by ongoing superposition and interaction of unsteadiness originating from physical cause of rotor blades revolution to stochastic vortical turbulent motion caused by turbulent boundary layers formed around moving fan blades, stationary fan duct cylinder, rotor-hub, stator blades, and other surfaces. Vorticity generated by rotor blades interacts with boundary layers of stator blades, generating higher-order stochastic periodicity. Methodology for statistical description of turbulence is to first ensemble average the flow to determine the average flow properties. In turbomachinery this is done by using the characteristic time period of flow behavior – the rotor blade passing period $1/BPF$. This procedure alone is not sufficient to completely resolve between these two physical causes in turbulent fan flow, and in this complex flow structure some physical unsteadiness associated with the rotor blades rotation will leak in the turbulent fluctuation signals, obtained by subtracting ensemble-averaged from the original flow signals. To reduce this deficiency of the ensemble-averaging signal processing alone, one could use digital filtering, as proposed in [4]. Such approach is adopted in this work. In order to better segregate between periodic mean flow and turbulence a digital filter procedure in frequency domain of turbulent velocity fluctuation signal is developed.

Experimental facility

Experimental facility consists of a high-speed axial ducted fan and a hot-wire anemometry system with a probe positioning mechanism.

High-speed axial ducted fan

Fan selected for this research work is the electric ducted fan by Great Planes – EDF 55 mm model originally designed for unmanned aerial vehicle, aircraft-vehicles. Operating point in this study is 27500 rpm, in free test-facility flow. Ratio of fan rotor diameter to the real-scale traffic-tunnel fan rotor is approximately 1:19. It is a high-speed axial ducted fan with 5-blade rotor and maximum rating of 50000 rpm. It is powered by Electri-

fly 20-40-3500 kV brushless AC motor, connected through an Electrify Silver Series Speed Control model SS-45 brushless ESC with a 11V DC power supply. Characteristic dimensions are: rotor duct diameter $2R_D = 54.1$ mm, tip clearance approximately 3-4% of blade height, rotor hub diameter $2R_H = 28$ mm. Flow measurements were performed at the duct exit section using a hot-wire probe, figs. 2, 3, and 4.

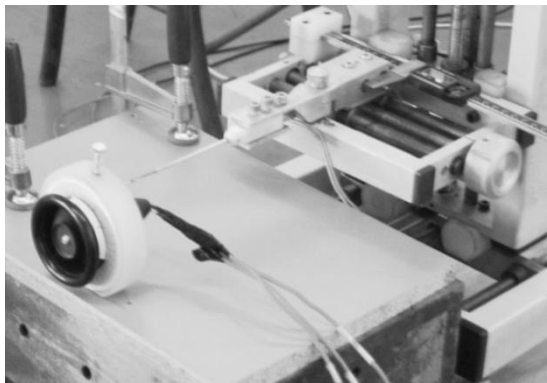


Figure 2. Fan testing facility

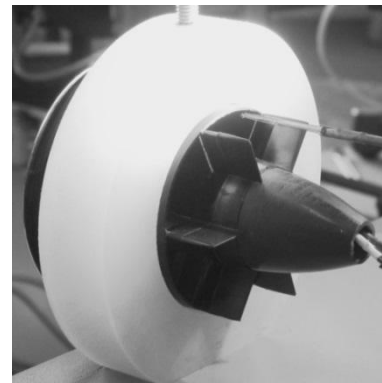


Figure 3. Measurement area of fan exit

Measurement space is confined in radial (span-wise) direction by rotor hub ring fitted over the hub holding extended blades (fig. 4), and fan duct inner diameter. Circumferentially, the flow exit area is limited by two neighboring stator blades and their extension blades, for a total of six pass-through spaces. All velocity components reported in this paper are in cylindrical co-ordinates: axial u , circumferential v_θ , and radial v_r . Probe was positioned along three different radiuses (fig. 4) fitted within the hub-shroud annulus space: $R_P = 16.2$, 21.2 , and 26.2 mm. Corresponding dimensionless radial span: $R_P^* = (R_P - R_H)/(R_D - R_H)$ values are: 0.168, 0.552, and 0.935. The circular angle co-ordinate measured in clockwise direction was varied in 2° increments between measurements, allowing 25-28 measurement points of the probe, depending on the radial span. All measurements in this work were repeated at identical probe tip positions with a 90° -rotated probe to obtain all three velocity components. For accurate positioning of the probe, a 3-axis thread-guide positioning system was used (fig. 2) allowing ± 0.01 mm resolution of probe displacements. To facilitate the probe re-positioning in circular 2° increments along selected radius, the fan duct was fitted in a machined housing attached to the test table. This allowed the fan duct to be rotated around its axis while the fan remains axially centered. Radial dependence of flow properties was measured along three different radial directions (fig. 4): mid-pitch and two near-wall directions, near the stator extended blades. Dimensionless stator-pitch angle is $\theta_p^* = \theta_p/\theta_{max}$, where θ_p angle spans between two neighbor stator blade surfaces. Values of θ_p^* for these three measurements of spanwise profile were: 0.052, 0.5, and 0.948. Probe was then repositioned using the guide mechanism alone, in 1 mm radial increments, for a total of eleven measurement points per pitch value.

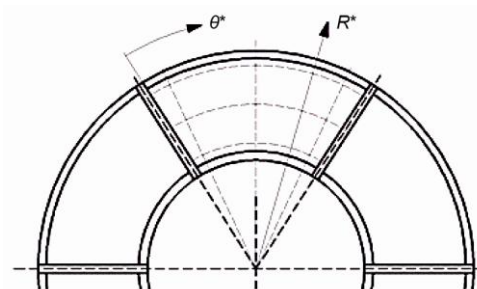


Figure 4. Measurement pitch-span window

Two-sensor hot-wire probe anemometry measurement system

A two-sensor hot wire X-probe with added pair of near-wall positioning pins, shown in fig. 5, was developed specifically for measurements of this kind. Prong spacing is 0.5 mm, platinum + 10% rhodium alloy sensors length is 0.71 mm and spanwise distance between two pairs of prongs is 0.3 mm. The details about probe construction and calibration can be found in [5-7], where probes of similar configuration and the calibration procedure are presented. Probe is heated by a constant temperature anemometer circuits designed by AA Lab Systems at a 1.4 overheat ratio, corresponding to approximately 290 °C sensor temperature, which provides reasonable sensitivity with minimal sensor thermal contamination. Frequency response of the system, for velocities in the range studied in this paper, was around 20 kHz. Signals were amplified using a 2nd stage amplifier of the anemometer unit, along with an analog filter built in the circuit and adjusted to filter out the very-high frequency noises.

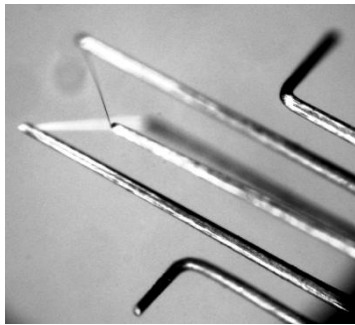


Figure 5. A 2-sensor hot wire X-probe

System was calibrated using laboratory wind tunnel producing a steady air nozzle flow in the desired velocity range of 23-50 m/s, upon initial measurements of spanwise velocity components, it is found that variation of yaw angle in the range of $\pm 15^\circ$ was sufficient, with most of the data within $\pm 10^\circ$. According to [8] the influence of the neglecting of one of the cross-stream velocity components on the accuracy of streamwise velocity component, is negligible. Probe calibration accuracy estimated by comparison of induced and measured velocity values is below 0.5%, for most of the measurement positions along this range. The RMS of measurement-system noise signal was acquired, and noise-induced velocity error estimated to be of the order under ± 0.03 m/s in our velocity measurement range. Ambient temperature variations during the carried experiments were within ± 0.4 °C. This corresponds to a velocity measurement error approximately within $\pm 0.5\%$, which is of the same order as the calibration accuracy of the system and is consistent with the results presented in study [9]. For this reason temperature correction procedure was not performed.

In order to determine the optimal sampling rate, the signal was sampled with 100 kHz which is upper limit of our AD convertor. Analyzing the velocity signal spectra it was determined that there is no significant energy in the flow at the frequencies above 20 kHz, which was the upper limit of our anemometry system. Optimal recording period of 15 seconds was assessed by analyzing its influence on some statistical and spectrum features of flow turbulence properties. It is a fairly long signal length (1.5 million samples), *i. e.* approximately 6875 complete fan rotor revolutions.

Signal processing procedure

Ensemble-averaging procedure

As mentioned previously and reported in references [3, 10, 11] the ensemble-averaging technique was used to process the velocity signal as the first step in resolving phase-averaged mean-flow from turbulence. It operates over the original signal in the time domain and can be defined as a mean-value filtering applied over a phase-coherent set of signal samples. The distance between the samples within each set is determined by the main pe-

riod of the signal, *i. e.* the blade passing period between two successive rotor blade passes in the stationary reference frame. In the work presented here, ensemble-averaging filter operates over a window of N_p rotor blade passing periods, and slides along the original velocity signals. The window is symmetrically centered around the current time moment. The procedure computes the ensemble-averaged mean value over a total number of $N_p + 1$ phase-coherent samples, and is denoted by $\tilde{u}(t)$, where tilda-hat sign is used trough this paper to denote ensemble-averaged quantities. Original velocity $u(t)$ is thus a sum of the ensemble-averaged $\tilde{u}(t)$ and the fluctuating component $u'(t)$:

$$u(r, \theta, z, t) = \tilde{u}(r, \theta, z, t) + u'(r, \theta, z, t) \quad (1)$$

$$\tilde{u}(r, \theta, z, t) = \frac{1}{N_p + 1} \sum_{i=-N_p/2}^{N_p/2} u(r, \theta, z, \tilde{t})_i, \quad \tilde{t} = t + \frac{1}{BPF} i \quad (2)$$

or in rotor-phase denotation:

$$\tilde{u}(r, \theta, z, \varphi) = \frac{1}{N_p + 1} \sum_{i=-N_p/2}^{i=N_p/2} u(r, \theta, z, \gamma)_i, \quad \gamma = \varphi + \frac{2\pi}{N_B} i \quad (3)$$

By test averaging a flow velocity signal, a period of $N_p = 300$ blade passes was selected for processing all velocity, *i. e.* 60 complete rotor revolutions or approximately 0.131 seconds of real flow time at $RPF = 458$ Hz rotor frequency, and the blade passing frequency $BPF = 2290$ Hz. This is consistent with the findings on recommended minimum number of ensemble periods with respect to total turbulence intensity, presented in study [11], on axial fan measurements with hot wire probes. The fast fourier transform (FFT) signal of energy spectrum of ensemble-averaged velocity will show the characteristic periodic pattern dominating at BPF , but will pass some higher order harmonics as well. Time averaged (mean flow) velocity is related to $\tilde{u}(t)$ as: $\bar{u} = \tilde{u}(t)$.

Filtering in the frequency domain

Complex structure of fan turbulence results from superposition of physically originated periodicity (rotor revolution) to turbulent motion in the boundary layers and rotor wakes. Fluctuating component, $u'(t)$ obtained by ensemble-averaging contains different periodicities. Ensemble-averaging leaks the lower-order physical periodicity directly related to the rotor blade rotational motion to the velocity fluctuation signal. This RPF (and BPF) periodicity can be removed from the turbulent fluctuation by filtering.

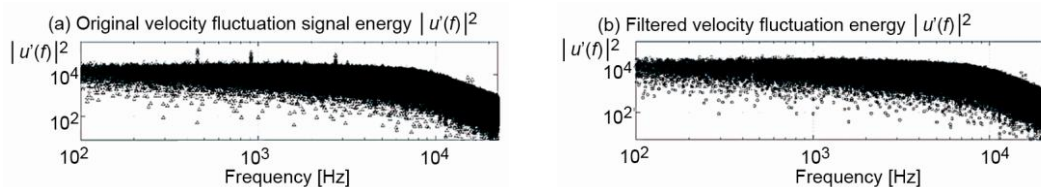


Figure 6. Velocity fluctuation signal energy $|u'(f)|^2$; (a) original, (b) filtered

Using harmonic analysis and FFT of $u'(t)$, energy spectral density $|u'(f)|^2$ of typical obtained velocity fluctuation signal, fig. 6, will show leaked lower order harmonics as re-

peated abrupt narrow energy peaks lying exactly at integer multiples of rotor (and blade passing) frequencies: $nRPF$ ($n = 1, 2, 3...$), and decaying in amplitude. At probe frequency response (20 kHz) signal energy is approximately 10^4 times lower than value at DC. The $nRPF$ harmonics up to ten times the blade passing frequency, *i. e.* $10 BPF = 50 RPF = 22920$ Hz where annulated using an iterative procedure. Filtered $u'(f)$ signal, which aims to represent the stochastic turbulence only, is returned to the time domain by inverse FFT. This procedure is used for all turbulence processing of measured data. Time-consuming computation of previous procedure was substantially sped up by a factor of over 80+, utilizing a 8-core multi-core central processing unit (CPU) and parallel computing of the code under MATLAB, compared to a CPU time for single processor execution of the same code.

Experimental results and discussion

Time-averaged flow

Time-averaged velocity components: \bar{u} , \bar{v}_r , \bar{v}_t are given in figs. 7(a)-(c). Different curves correspond to probe dimensionless span: $R_p^* = (R_p - R_H)/(R_D - R_H) = 0.169, 0.55$, and 0.935 . Values are plotted against one stator pitch dimensionless angle θ_p^* , which increases clockwise between stator blades from 0 to 1, while viewing from a downstream (z-tip) position, towards the fan, fig. 4. Rotor revolution appears also clockwise from this viewpoint. The $\theta_p^* = 0$ and one positions are taken at stator blade wall surfaces. Angle increment between measurement points was 2° , or $\Delta\theta_p^* = 0.0359$. The outmost (near-blade) measurement probe positions were approximately 1.23 mm from the stator blade wall.

As expected, highest axial velocity is registered along the mid-value radius $R_p^* = 0.552$. Maximum value is between 0-0.5 pitch value. Curvature of stator blades is designed to straighten the flow within the fan duct so the flow is axially accelerated. Tangential velocity changes sign in the $\theta_p^* \rightarrow 1$ area. This behavior is consistent and is a result of duct and stator blades boundary layers displacement-behavior.

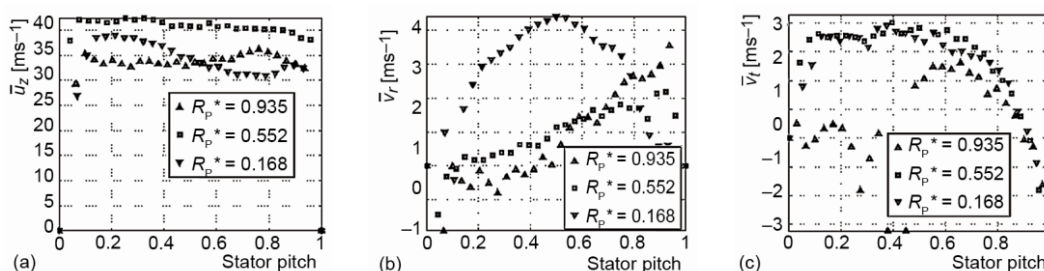


Figure 7. (a) Time-averaged axial velocity, \bar{u} , (b) Time-averaged radial velocity, \bar{v}_r , (c) Time-averaged tangential velocity, \bar{v}_t

Such influence on radial component is propagated more towards the midpoint θ_p^* value as radius increases, as a result of the duct boundary layer. Near the fan hub radial component has its highest values, reaching maximum in the midpoint of stator pitch, away from stator blades. Such distribution is also promoted by the existence of a streamlined ring, fig. 3 which holds the extension of stator blades, downstream of the duct exit. This ring extends from the hub surface (by 1.15 mm or $R_p^* = 0.088$, approximately 5.5 mm downstream of the probe tip), and will promote radial component and boundary layer separation. Radial distribution of time-averaged velocities is obtained for stator pitch values: 0.052, 0.5, and 0.948, re-

spectively, held constant during respective radial probe displacements. Outmost positions are approximately 2.87° away from stator blade wall. Spanwise probe displacement was 1 mm or $\Delta R_p^* \sim 0.077$, in span range: 0.168-0.935. Results are shown in figs. 8(a)-(c). Axial component reaches its maximum of approximately 41.6 m/s at about $R_p^* = 0.7$ near the lower stator pitch value blade. Maximum values of tangential component ~ 5 m/s are reached at mid-pitch at ~ 0.77 span value. Tangential component's sign stays in accordance with rotor revolution along the stator pitch value except for the outmost + pitch, and near the duct.

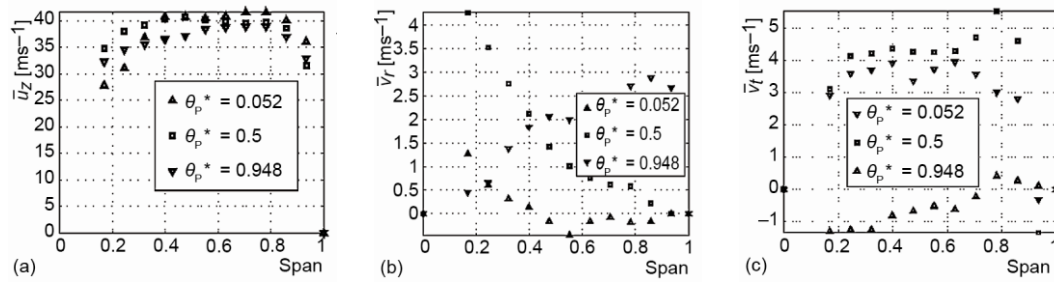


Figure 8. (a) Time-averaged axial velocity, \bar{u}_z , (b) Time-averaged radial velocity, \bar{v}_r , (c) Time-averaged tangential velocity, \bar{v}_t

Turbulence and transient properties

To conduct a detailed CFD analysis of tunnel air and pollutant flow, the fan flow information is required. Besides the mean-value of fan velocity components discussed in previous chapter, the other turbulence properties as turbulence kinetic energy/intensity, and dissipation rate are desirable. For more advanced turbulence modeling, additional experimental information on stresses is valuable in order to check the quality of numerical approach. In addition, in order to investigate further tunnel fan improvements, as discussed in recent studies [3], and optimize CFD approaches for accuracy, experimental knowledge of more detailed physical quantities like Reynolds stresses, flow length scales and turbulent kinetic energy (TKE) production rate is desirable.

Definitions used to compute TKE denoted as k , turbulence departure to anisotropy DA , and the turbulence intensity Tu , are given in eq. (4), respectively. Integral length scale for turbulent flow estimates the size of the largest eddies, the definition is given in eq. (5). Auto-correlation function $R(\tau)$ is computed up to its first zero amplitude, as suggested by the study in [12].

$$(a) \quad k = \frac{1}{2} \left(u'^2 + v_r'^2 + v_t'^2 \right), \quad (b) \quad DA = \frac{2u'^2}{v_r'^2 + v_t'^2}, \quad (c) \quad Tu = \frac{\sqrt{\frac{1}{3} \left(u'^2 + v_r'^2 + v_t'^2 \right)}}{\sqrt{\bar{u}^2 + \bar{v}_r^2 + \bar{v}_t^2}} \quad (4)$$

$$(a) \quad L = U \int_0^\infty R(\tau) d\tau, \quad R(\tau) = \frac{\overline{u'(t)u'(t+\tau)}}{\overline{u'^2}}, \quad (b) \quad \mathbf{R}_{ij} = -u'_i u'_j, \quad (5)$$

$$(c) \quad \mathbf{P}_{ij} = -u'_i u'_j \frac{\partial \bar{u}_i}{\partial x_j}$$

Span vs. time distribution of flow properties is constructed for $\theta_p^* = 0.5$. Ensemble-averaged axial, radial, and tangential velocities over two blade passing periods (BPP), are pre-

sented in figs. 9(a)-(c). Yaw and pitch flow angle values, $\tilde{\alpha}$ and $\tilde{\beta}$, are shown in figs. 10(a) and (b). The TKE, k , and its departure to anisotropy DA , are presented in figs. 11(a) and (b). Turbulence is fairly isotropic over BPP periods, with DA value of 0.5-2.5% in most of the span space, except for phases when rotor wakes are convected downstream and approach the probe with anisotropy values over 4%. Maxima of dimensionless TKE – k (under $\sim 0.3\%$), correspond to these phases. Same is true for quantities like Reynolds stresses. Axial-tangential Reynolds stress, \mathbf{R}_{uv} , spanwise ($\theta_p^* = 0.5$) distribution over 2-D BPP periods is presented in fig. 12, in its physical SI units. Integral length scale of flow computed also over central-pitch span is presented in the fig. 11(c). It shows average value of largest flow scales of ~ 2 mm, or $\sim 15\%$ of rotor blade's span. Measurement system allowed to measure five out of six independent members of the Reynolds stress tensor, \mathbf{R}_{ij} . Distribution of dimensionless mean-value Reynolds stresses vs. radial span for central pitch $\theta_p^* = 0.5$, and pitch distribution for $R_p^* = 0.552$ span, are presented in fig. 13(a) and (b), respectively. Mean value is computed by time-averaging over 6000 BPP (1200 rotor turns). Stresses are non-dimensionalized by rotor tip speed U_{tip}^2 ($U_{tip} = 78$ m/s). The TKE production rate tensor \mathbf{P}_{ij} terms, time-averaged analogous to \mathbf{R}_{ij} , are shown in figs. 14(a) and (b). For convenience, values shown are in its physical SI units.

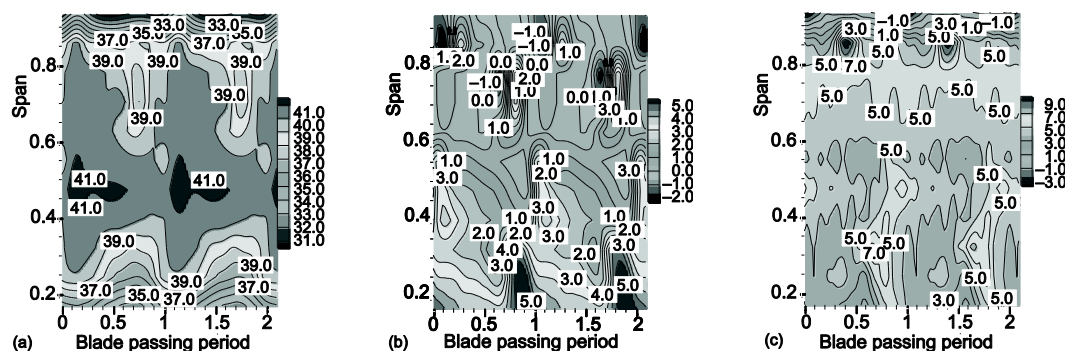


Figure 9. (a) \tilde{u} , (b) \tilde{v}_r , (c) \tilde{v}_t

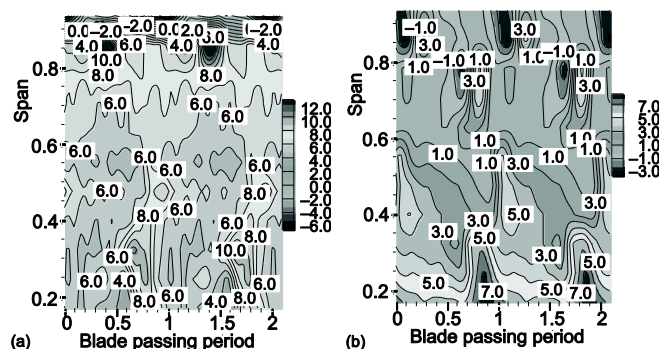


Figure 10. (a) Yaw angle, $\tilde{\alpha}$, (b) Pitch angle, $\tilde{\beta}$

Using available 2-sensor X-probe data and numerical differentiation, it was possible to compute maximum four members of the \mathbf{P}_{ij} tensor: two in span-wise distribution, and other two members in pitch-wise directions, fig. 14. Transient nature of velocity is presented by

computing ratios of instantaneous and ensemble-averaged velocities – vs. their corresponding time averages. This is done for axial and tangential velocity: $u/\bar{u}, \tilde{u}/\bar{u}$ in fig 14, and $v_t/\bar{v}_t, \tilde{v}_t/\bar{v}_t$ in fig. 16. Both figs. are computed for $\theta_p^* = 0.5$ and three different span probe positions: (a) near-duct, (b) mid-span, and (c) near-hub. Turbulent boundary layers increase these ratios considerably as fan duct and rotor hub surfaces are approached by probe tip.

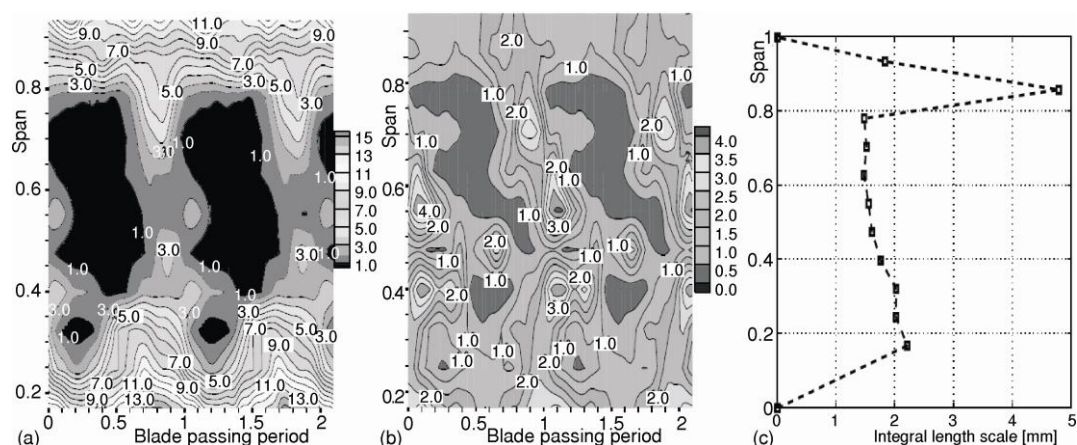
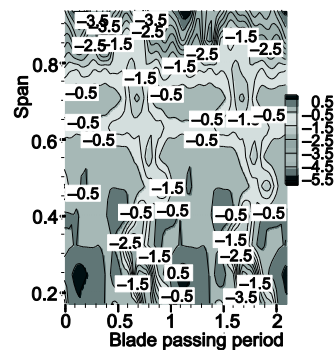


Figure 11. (a) TKE – k [m²s⁻²], (b) DA [%], (c) integral scale [mm]

Turbulence intensity, Tu [%] exiting the fan, is computed according to definition proposed for turbomachinery flows, [4], *i. e.* eq. 4(c). Spanwise distribution for central pitch as a function of dimensionless time is presented in fig. 17. From a tunnel-aerodynamics point of view, this turbulence intensity will be superimposed to periodic (physical) unsteadiness presented by ensemble-averaged flow, previously seen on figs. 15 and 16.

Dimensionless thrust coefficient of the analyzed fan, C_T defined:

$$C_T = \frac{T}{\rho D^4 n^2} \quad (6) \quad \text{Figure 12. } R_{uv} = -u'v'_t \text{ [m}^2\text{s}^{-2}\text{]}$$



where n [rps], D [m] is the rotor diameter, T [N] – the static thrust is determined by measuring the fan static thrust force [1], fig. 18. Fan thrust was measured on a test table device designed for this purpose. The fan is held on one side of a balance lever, pivoting on a horizontal roller-bearing supported axle attached to the test table, and thrust reaction is measured by electronic scale on the opposite side.

Ducted fan total thrust can be also determined using a common formula [2, 3]:

$$T = \rho A w(w - w_\infty) \quad (7)$$

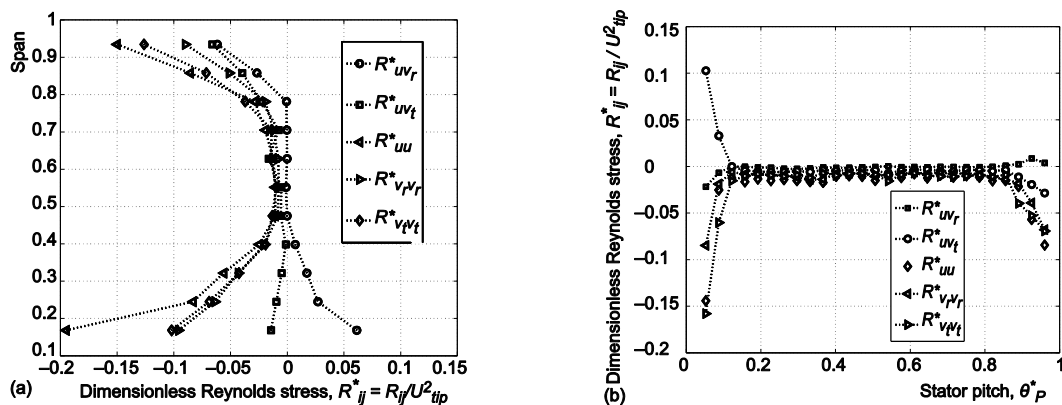


Figure 13. Mean-value of ensemble-averaged dimensionless Reynolds stresses [%] $R_{ij} = -u'_i u'_j / U_{tip}^2$; (a) spanwise-distribution for $\theta_p^* = 0.5 = \text{const.}$, (b) pitch-distribution for $R_{P^*} = 0.552 = \text{const.}$

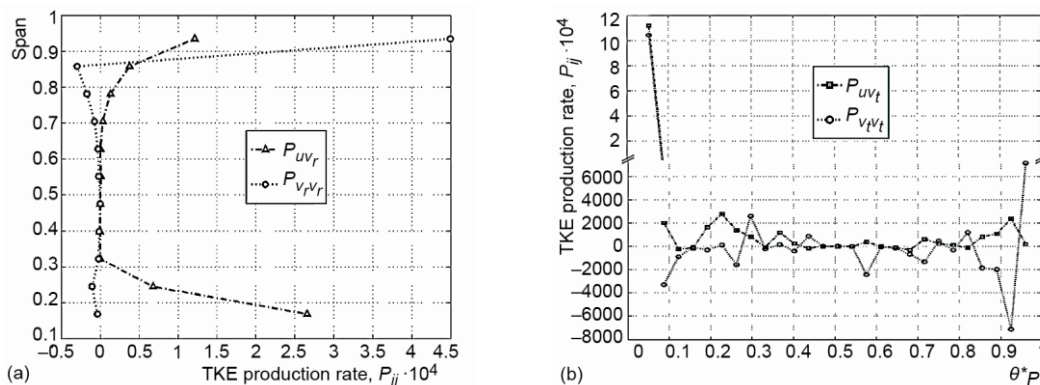


Figure 14. Mean value of ensemble-averaged turbulent kinetic energy production rates P_{ij} [$\text{m}^2 \text{s}^{-3}$]; (a) spanwise-distribution for $\theta_p^* = 0.5 = \text{const.}$, (b) pitch-distribution for $R_{P^*} = 0.552 = \text{const.}$

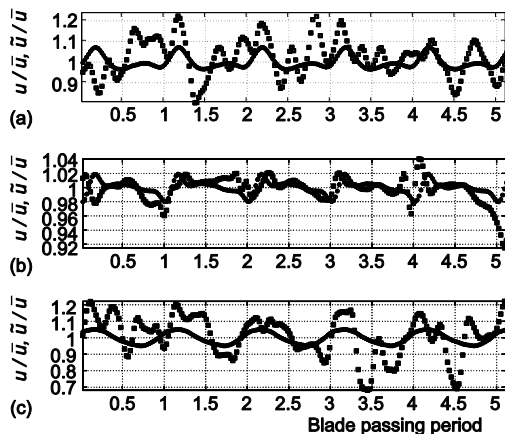


Figure 15. Ratio of \tilde{u}/\bar{u} (\square), $\tilde{\tilde{u}}/\bar{\tilde{u}}$ ($*$), at points $R_{P^*} =$ (a) 0.168, (b) 0.552, (c) 0.935; $\theta_p^* = 0.5 = \text{const.}$

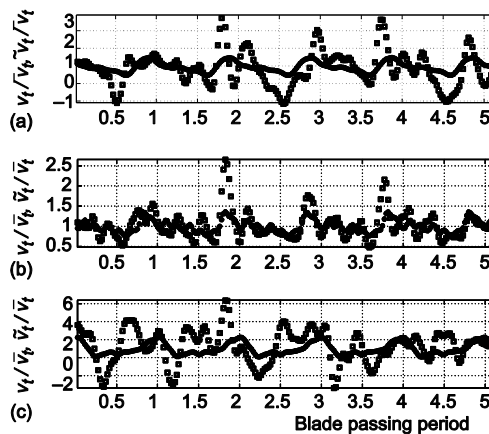


Figure 16. Ratio of v_r/\bar{v}_r (\square), $\tilde{v}_r/\bar{\tilde{v}}_r$ ($*$), at points $R_{P^*} =$ (a) 0.168, (b) 0.552, (c) 0.935; $\theta_p^* = 0.5 = \text{const.}$

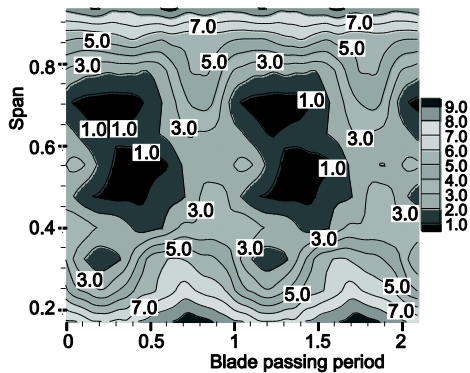


Figure 17. Turbulence intensity, Tu [%]

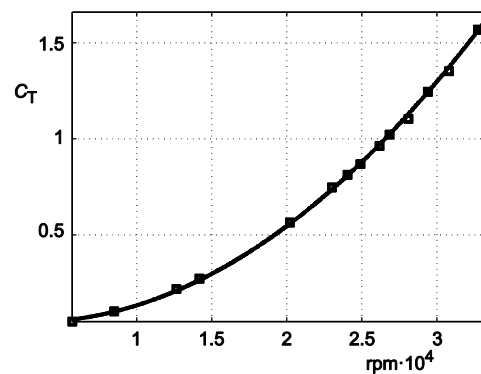


Figure 18. Dimensionless thrust coefficient

where w is the mean exit velocity. By numerical integration of the interpolated experimental axial exit velocity field, volume flow rate and a corresponding axial velocity mean-value of approximately $w \approx 34.6$ m/s at the studied rpm, is obtained. Computed total thrust eq. (7) based on this value, for static thrust conditions ($w_\infty \approx 0$), is in a very good agreement with the measured value, fig. 18, at the corresponding rpm value.

Some results can be compared to [4, 12] where axial fan flow was investigated in detail using hot wire anemometry. In [4] a ducted 600 mm axial fan flow was determined 129% of blade span downstream of the rotor, using a 3-sensor probe. In [13] a 360 mm axial fan without a duct cylinder was examined. Exit flow was measured at 9% of blade span downstream of the rotor using a 2-sensor probe. Both references analyze fans without downstream stator blades, present in the fan design studied here. As explained here, the flow measurement was performed at 176% of blade span downstream of the rotor. These elements prevent a direct comparison of results with respect to geometry.

Transient nature of ensemble-averaged velocity and turbulent properties show similar character: axial velocity component \tilde{u}/\bar{u} ratio of this study is $\sim 2\%$ at midspan increasing to 8% near walls, while it is 5% at midspan in [4], and in the 4-25% spanwise range in [13]. The spanwise average integral length-scale of flow is 15% and 13.5% of rotor blade height, in this study and in [4], respectively. Turbulence intensity is in the 1-9% range in this study, and 1-11% in [4]. Reference [13] reports relative turbulence per velocity component – axial component comparison at the same span probe position ($R_p^* = 0.786$) shows similar periodic character and amplitude range: 2-5%.

Comparison reveals reduced levels of turbulence expressed through TKE and \mathbf{R}_{ij} for the fan studied here. This can be attributed to the effect of fan duct attenuation of secondary flow component's turbulence further downstream of the rotor in [4] and this study. For example, TKE is reported in [13] and it's dimensionless spanwise rotor-phase distribution is in the 0.21-0.43% range, while it is up to $\sim 0.25\%$ in this study. The \mathbf{R}_{ij}^* tensor main diagonal dimensionless values at the same span positions (near-hub and near-shroud) are: $R_{uu}^* = 0.2/0.15\%$, $R_{v_r v_r}^* = 0.1/0.1\%$, and $R_{v_t v_t}^* = 0.1/0.125\%$, in this study, and values reported in [13] are: $R_{uu}^* = 0.14/0.29\%$; $R_{v_r v_r}^* = 0.07/0.29\%$, and $R_{v_t v_t}^* = 0.25/0.29\%$.

Conclusions

Results of hot-wire anemometry experimental analysis of high-rpm axial ducted fan turbulent flow are presented. Ensemble-averaged fields and time-averaged profiles of flow ve-

locities, yaw and pitch angles, integral flow scales, turbulent kinetic energy, available Reynolds stresses, turbulent kinetic energy production rates, and the dimensionless thrust coefficient, are determined for this type of fan by processing experimental data. The transient character of ensemble averaged flow properties is determined in detail and presented. Mean value profiles of Reynolds stresses and turbulent kinetic energy production rates are presented for central stator pitch span-wise, and mid-span pitch distributions. Axial exit velocity field is interpolated and resulting fan volume flow rate and fan static thrust is determined using common relation (7) against the fan's static thrust measurements. Some turbulent properties are compared results in similar studies of axial fan flow.

The obtained results can be used in collaboration with CFD to further investigate both the fan flow and the entire tunnel ventilation system. The turbulent fan flow data obtained by processing experimental measurements can be used as a boundary condition for CFD computation of tunnel flows. Several factors and possible improvements – overall tunnel's ventilation energy and vehicle-emitted pollutant transport efficiency, the incident fire scenarios, can be further analyzed from this. Results can be compared to our model experiments [1], where these fans are utilized. Fan induced swirl and turbulence effect on the resulting tunnel flow, pollutant transport, and the resulting energy and ventilation efficiency can be assessed. In addition, a more accurate evaluation of 1-D numerical models for tunnel ventilation design is possible.

Presented data are valuable for benchmark testing axial fan CFD computation performance and the associated turbulence modeling accuracy. Tunnel fan improvements could be further investigated by CFD, utilizing a similar methodology presented in [14] and the tunnel-model facility presented in [1], available in our laboratory.

Acknowledgments

This work is financially supported by the Mechanical Engineering Faculty, University of Montenegro, and research project grant of the Ministry of Science of Montenegro.

Nomenclature

A – surface, [m²]
 BPF – blade passing frequency, [Hz]
 C_T – thrust coefficient, [-]
 D – rotor diameter, [m]
 DA – departure to anisotropy, [-]
 i – value sample index
 k – turbulent kinetic energy, [m²s⁻²]
 L – integral length scale, [m]
 n – revolution speed, [rps⁻¹]
 \mathbf{P}_{ij} – TKE production rate, [m²s⁻³]
 R_D, R_H – radius of duct and hub, [m]
 R_p^* – probe radius, [-]
 RPF – rotor passing frequency, [Hz]
 \mathbf{R}_{ij} – Reynolds stress tensor, [m²s⁻²]
rpm – revolutions per minute

rps – revolutions per second
 T – fan static thrust force, [N]
 T_u – turbulent intensity, [-]
 t – time, [s]
 \tilde{t} – time of i^{th} sample in a ph. aver. set
 U – average velocity, [ms⁻¹]
 w – mean value exit velocity, [ms⁻¹]

Greek symbols

$\tilde{\alpha}, \tilde{\beta}$ – yaw and pitch angles, [°]
 γ – rotor phase, [rad]
 ρ – density, [kgm⁻³]
 θ_p^* – angle/stator pitch, [-]
 φ – stator phase, [rad]

References

- [1] Šekularac, B. M., Vukoslavčević, V. P., One Approach to Experimental and Numerical Investigation of Longitudinally Ventilated Road Tunnels, *Proceedings, ICTTE Conference*, Belgrade, 2012

- [2] Tarada, F, Brandt, R., Impulse Ventilation for Tunnels – A State of the Art Review. *Proceedings*, 13th International Symposium on Aerodynamics and Ventilation of Vehicle Tunnels, New Brunswick, N. J., USA, 2009
- [3] Rudelgass, H., Barbeta, C., An Improved Jet Fan, *Tunnels and Tunneling International* (2012), July, pp. 58-60
- [4] Oro, J. M. F., *et al.*, Turbulence and Secondary Flows in an Axial Flow Fan With Variable Pitch Blades, *Journal of Fluids Engineering*, 130 (2008), 4, pp. 041101-1
- [5] Vukoslavčević, P. V. Wallace, J., A 12-Sensor Hot-Wire Probe to Measure the Velocity and Vorticity Vectors in Turbulent Flow, *Meas. Sci. Technol.*, 7 (1996), 10, pp. 1451-1461
- [6] Moro, J. P., *et al.*, A Method to Calibrate a Hot-Wire X-Probe for Applications in Low-Speed, Variable-Temperature Flow, *Meas. Sci. Technol.*, 14 (2003), 7, pp. 1054-1062
- [7] Vukoslavčević, P., Petrović, D., Multiple Hot-Wire Probes – Measurements of Turbulent Velocity and Vorticity Vector Fields, Ph. D. thesis, Montengrin Academy of Sciences and Arts, Podgorica, Montenegro, 2000
- [8] Petrović, D. V., *et al.*, The Accuracy of Turbulent Velocity Component Measurements by Multi-Sensor Hot-Wire Probes: a New Approach to an Old Problem, *Experiments in Fluids* 34 (2003), 1, pp. 130-139
- [9] Kanevče, G., Oka, S., Correcting Hot-Wire Readings for Influence of Fluid Temperature Variations, *DISA Inf.15* (1973), 15, pp. 21-24
- [10] Uzol, O., *et al.*, Experimental Investigation of Unsteady Flow Field within a Two Stage Axial Turbomachine Using Particle Image Velocimetry, *Proceedings*, ASME TURBO EXPO 2002, Amsterdam. GT-2002-30664
- [11] Oro, F. J. M., *et al.*, Converged Statistics for Time-Resolved Measurements in Low-Speed Axial Fans Using High-Frequency Response Probes, *Experimental Thermal and Fluid Science*, 54 (2014), Apr., pp. 71-84
- [12] O'Neill, P. L., *et al.*, Autocorrelation Functions and the Determination of Integral Length with Reference to Experimental and Numerical Data, *Proceedings*, 15th Australasian Fluid Mechanics Conference, Sydney, Australia, 2004
- [13] Kergourlay, G., *et al.*, Experimental Investigation of the 3-D Unsteady Flow Field Downstream of Axial Fans, *Flow Measurement and Instrumentation*, 17 (2006), 5, pp. 303-314
- [14] Protić, Z., *et al.*, Novel Methods for Axial Fan Impeller Geometry Analysis and Experimental Investigation of the Generated Swirl Turbulent Flow, *Thermal Science*, 14 (2010), Suppl. 1., pp. S125-S139